



Modeling and analysis of hydrogen permeation in mixed proton–electronic conductors

Lin Li^{a,b,1}, Enrique Iglesia^{a,b,*}

^aDepartment of Chemical Engineering, University of California at Berkeley, Berkeley, CA 94720-1462, USA

^bDivision of Materials Sciences, E.O. Lawrence Berkeley National Laboratory, Berkeley, CA 94720, USA

Received 22 August 2002; received in revised form 20 January 2003; accepted 27 January 2003

Abstract

A rigorous model for hydrogen permeation through dense mixed conductors was derived using the formalism of non-equilibrium thermodynamics for various operating modes and process conditions. The concentrations of charge carriers were rigorously included in this model through defect equilibria with the chemical environment at each membrane surface and through balance equations and a virtual pressure formalism within the membrane. Hydrogen permeation rates through proton–electron–hole mixed conductors were simulated using this framework under open-circuit, short-circuited, and applied potential operating modes. The sensitivity of H₂ permeation rates to the reduction–oxidation potentials at each side of the membrane and to the membrane properties (e.g. electron/hole diffusivity, oxygen binding energy) was examined in terms of the mobility and concentration of each charge carrier in order to identify rate-limiting steps for H₂ transport. These simulations showed that electronic transport controls H₂ permeation rates in proton–electron–hole mixed conductors typically used for H₂ permeation, especially when hydrogen chemical potentials are significantly different in the two sides of the membrane. These electronic conduction limitations arise from a region of very low electronic conductivity within the membrane, caused by a shift in the predominant charge carriers from electron to holes with decreasing hydrogen chemical potential. Under these asymmetrical conditions, H₂ permeation rates increase more markedly when an external electron-conducting path is introduced than at lower chemical potential gradients. Such interplay between rate-controlling variables leads to complex effects of H₂ chemical potential gradients on permeation rates. The effects of intrinsic membrane properties on H₂ permeation were examined by systematic changes in the defect equilibrium constants. A decrease in oxygen binding energy, manifested in a stronger tendency for reduction of the oxide membrane material, leads to higher electron concentrations and to higher rates for open-circuit operation, during which electron conduction limits H₂ transport rates. © 2003 Elsevier Science Ltd. All rights reserved.

Keywords: Model; Simulation; Mass transfer; Membrane; Proton conduction

1. Introduction

Metal oxides with mixed ionic–electronic (ambipolar) conductivity have attracted considerable attention as dense membranes useful in separations, chemical reactors, and fuel cells. Most studies of ionic transport through dense oxides have focused on oxygen-permeable materials (Bouwmeester & Burggraaf, 1996), but high-temperature proton conductors have been known for some time (Iwahara, 1996; Nowick & Du, 1996; Kreuer, 1997, 1999, 2000; Norby, 1999). The

defect chemistry and the proton conductivity of these materials under electrochemical conditions has been studied, but few reports have addressed the ability of these materials to permeate hydrogen (Balachandran et al., 2001; Guan, Dorris, Balachandran, & Liu, 1998; Hamakawa, Hibino, & Iwahara, 2002; Li & Iglesia, 2001; Qi & Lin, 2000). As a result, kinetic and mechanistic descriptions of hydrogen permeation behavior through proton–electronic mixed conductors remain incomplete.

Some theoretical guidance is available from treatments of oxygen transport (Bouwmeester & Burggraaf, 1996), but the conditions and the relevant transport mechanisms differ significantly in these two systems. For example, both sides of oxygen transport membranes may be in contact with oxidizing streams. Under such conditions, the required electronic conduction is carried out by holes (p-type conduction). In

* Corresponding author. Department of Chemical Engineering, University of California at Berkeley, Berkeley, CA 94720-1462, USA. Tel.: +1-510-642-9673; fax: +1-510-642-4778.

E-mail address: iglesia@cchem.berkeley.edu (E. Iglesia).

¹ Current address: UOP LLC, 25 East Algonquin Rd., Des Plaines, IL 60017, USA.

contrast, H₂ permeation involves at least one side exposed to a reducing environment. This leads to very low hole conductivities, because hole concentrations in acceptor-doped perovskites decrease with decreasing oxygen thermodynamic activity. These reducing or asymmetric (reducing in one side and oxidizing in the other) conditions lead to changes in rate-determining charge carriers as a function of position within the membrane thickness. The characterization and prediction of the relevant rate processes require rigorous transport models of greater complexity than those needed for oxygen transport systems.

Recently, [Norby and Larring \(2000\)](#) reported a hydrogen permeation model for proton conductors. Their model describes the behavior of such systems for open-circuit conditions, in which no net current flows across the membrane and the electrical potential gradient equals the net chemical potential gradients for all charge carriers. Hydrogen flux equations were derived by assuming electron transference numbers of unity (conductivities much greater for electrons than for protons) and then expressing the flux as a function of the proton conductivity and the hydrogen partial pressure.

The dearth of permeation data remains a significant hurdle to the validation and improvement of available permeation models. Simulations based on the [Norby and Larring \(2000\)](#) model have not been compared with permeation data; also, this model is useful only for materials with high electronic conductivity, for which the hydrogen flux is controlled only by proton transport. Yet, H₂ permeation data indicate that electronic conduction is a kinetically relevant step in the overall transport process ([Balachandran et al., 2001](#); [Guan et al., 1998](#); [Li & Iglesia, 2001](#); [Qi & Lin, 2000](#)). Proton conduction through dense membranes involves proton migration via hopping of hydrogen atoms among lattice oxygen atoms within the structure of perovskite materials, without concurrent motion of oxygen anions. Indeed, immobile oxygens, generally associated with electronic insulators, are essential in order to avoid oxygen migration and membrane over-reduction during hydrogen permeation ([Bouwmeester & Burggraaf, 1996](#); [Tuller, 1981](#); [Smyth, 1992](#)). Also, hydrogen separation membranes must be operated at relatively low temperatures (< 1000 K) in order to prevent oxygen permeation and membrane reduction. Electronic conductivities show higher activation energies than the corresponding conductivities for protons ([Tuller, 1981](#); [Smyth, 1992](#)); as a result, electron transport rates are typically lower than proton transfer rates, leading to electron transference numbers significantly less than unity.

In all previous mass transfer models of mixed conductors ([Norby & Larring, 2000](#); [Guan et al., 1998](#); [Qi & Lin, 2000](#)), hydrogen permeation has been described in terms of proton and electronic conductivities that are taken either as constant across the membrane cross-section or as empirical functions of H₂ partial pressure. In reality, these conductivities, as defined, depend not only on the transport properties of the solid (i.e., charge carrier mobility), but also on the concentrations of each charge carrier. These concentrations,

in turn, depend on the chemical composition of the contacting gas phase and on the position across the membrane thickness, because of the prevalent chemical potential gradients responsible for net mass transport. As a result, conductivities have retained a qualitative character in all previous attempts at rigorous descriptions of net transport rates, because they do not reflect merely the intrinsic properties of the materials, but depend also on conditions, the required details of which are not always reported or even measured in parallel experiments. Recently, [Huggins \(2001\)](#) discussed charge carrier transport inside solid electrolytes by using defect equilibrium diagrams, but his analysis focused on electrical properties of solid electrolyte material, and not on the rate of proton transfer processes.

We propose here a comprehensive model designed to describe hydrogen permeation behavior in proton–electron mixed conductor membranes. Such models, when accurate and rigorous, provide essential guidance in the design and understanding of mixed conducting materials. The model proposed uses the formalism of non-equilibrium thermodynamics in order to provide rigorous and accurate descriptions of transport processes as a function of chemical environment and operating modes. The identity of the limiting charge carriers is specifically probed with the objective of guiding the search for materials that overcome transport bottlenecks in currently available conductors.

2. Mass transfer model for proton–electronic mixed conductor membranes

In mixed conductors, chemical and electrical potential gradients co-exist and they act as the driving force for mass transport. Along the dimension of net transport (x = membrane thickness), mass transfer rates per cross-sectional area (fluxes) for component k are given by ([Bouwmeester & Burggraaf, 1996](#))

$$J_k = -\frac{c_k D_k}{RT} \left(\frac{d\mu_k}{dx} - z_k F \frac{d\phi}{dx} \right). \quad (1)$$

In Eq. (1), the first and second terms represent transport driven by chemical and electrical potential gradients, respectively. If we choose component 1 as the basis component, the electrical potential gradient $d\phi/dx$ can be expressed as a function of the chemical potentials of all other charge carriers. The flux for species of 1 then becomes (Appendix I)

$$J_1 = \frac{c_1 D_1}{A} \frac{I}{F} - \frac{\sum_{k=2}^n z_k^2 c_k D_k}{A} \frac{c_1 D_1}{RT} \frac{d\mu_1}{dx} + \frac{c_1 D_1}{A} \sum_{k=2}^n \frac{c_k D_k z_k}{RT} \frac{d\mu_k}{dx}, \quad (2)$$

where

$$A = \sum_{k=1}^n z_k^2 c_k D_k. \quad (3)$$

Eq. (2) describes fluxes for each charge carrier as a function of both their chemical potential gradient and those for all other species. This gives rise to a significant practical hurdle, because it is difficult to measure the chemical potential of each charge carrier within the membrane material, as required for the solution of Eq. (2). Thus, we must describe these potentials as a function of the concentrations and chemical potentials of the gas-phase species (e.g., H_2 , H_2O , O_2) in contact with each side of the membrane. If both sides are brought in contact with the same gas mixture, the concentrations of all charge carriers will ultimately reach equilibrium with this gas phase, and their concentrations and chemical potentials at each point will depend only on the thermodynamics of the gas–solid reactions responsible for these equilibria. In proton–electron–hole mixed conductors, charge carriers include protons (OH^\cdot), electrons (e'), electron holes (h^\cdot) and vacancies ($V_{\bar{O}}$)

For typical proton conductors, such as $SrCe_{0.95}Yb_{0.05}O_{3-x}$, the gas–solid reactions can be described by the following stoichiometric equations (Iwahara, 1996; Schober, Schilling, & Wenzl, 1996):



These three reactions, however, are not independent, because the H_2O , H_2 and O_2 partial pressures must satisfy the thermodynamics for the reaction



At each point within the membrane material, the charge carrier concentrations can be considered to be in quasi-equilibrium with a set of virtual partial pressures of H_2 , O_2 , and H_2O (π_j). These virtual partial pressures act as surrogates for the chemical potentials of these respective species at each point within the solid (Boudart & Djega-Mariadassou, 1984). Therefore, the flux equations can be expressed as functions of gradients in the virtual pressures of hydrogen and water (Appendix A):

$$j_{OH} = \frac{\varepsilon_{OH}}{\lambda} i - \frac{\varepsilon_{OH}}{2\lambda} \left[(\varepsilon_h \gamma_h + \varepsilon_e \gamma_e) \frac{d \ln(\pi_{H_2})}{d\xi} + 4\varepsilon_V \gamma_V \frac{d \ln(\pi_w)}{d\xi} \right], \quad (8)$$

$$j_V = \frac{2\varepsilon_V \gamma_V}{\lambda} i + \frac{\varepsilon_V \gamma_V}{\lambda} \left[(\varepsilon_h \gamma_h + \varepsilon_e \gamma_e + \varepsilon_{OH}) \frac{d \ln(\pi_w)}{d\xi} - (\varepsilon_h \gamma_h + \varepsilon_e \gamma_e) \frac{d \ln(\pi_{H_2})}{d\xi} \right]. \quad (9)$$

Eqs. (8) and (9) are general flux equations that describe mass transport in mixed conductor membranes. These flux equations can be simplified to obtain expressions for

specific membrane compositions, chemical environments, and operating conditions, as we describe in detail below.

2.1. Open-circuit conditions

For open-circuit conditions ($I = 0$), the fluxes of protons and vacancies are given by

$$(j_{OH})_{open} = -\frac{\varepsilon_{OH}}{2\lambda} \left[(\varepsilon_h \gamma_h + \varepsilon_e \gamma_e) \frac{d \ln(\pi_{H_2})}{d\xi} + 4\varepsilon_V \gamma_V \frac{d \ln(\pi_w)}{d\xi} \right], \quad (10)$$

$$(j_V)_{open} = \frac{\varepsilon_V \gamma_V}{\lambda} \left[(\varepsilon_h \gamma_h + \varepsilon_e \gamma_e + \varepsilon_{OH}) \frac{d \ln(\pi_w)}{d\xi} - (\varepsilon_h \gamma_h + \varepsilon_e \gamma_e) \frac{d \ln(\pi_{H_2})}{d\xi} \right]. \quad (11)$$

At steady state, j_{OH} and j_V must be constant at every point within the membrane and the above equations can be re-arranged to give (Appendix A)

$$\frac{d(\ln \pi_{H_2})}{d\xi} = \frac{4j_V}{(\varepsilon_h \gamma_h + \varepsilon_e \gamma_e)} - \frac{2j_{OH}}{\varepsilon_{OH}} \frac{\varepsilon_h \gamma_h + \varepsilon_e \gamma_e + \varepsilon_{OH}}{\varepsilon_h \gamma_h + \varepsilon_e \gamma_e}, \quad (12)$$

$$\frac{d(\ln \pi_w)}{d\xi} = \frac{j_V}{\varepsilon_V \gamma_V} - \frac{2j_{OH}}{\varepsilon_{OH}}. \quad (13)$$

With appropriate boundary conditions, Eqs. (12) and (13) can be integrated to obtain j_V and j_{OH} . The charge carrier concentrations involved in these two equations can be obtained from the interactions between gas-phase molecules and the membrane surface, as described in Section 3.

2.2. Short-circuited conditions

For short-circuited conditions, potential differences across the membrane become negligible because a connecting external conductor provides a path of negligible resistance for electron transport (i.e. $d\phi/dx = 0$). Then, we obtain from Eq. (1)

$$(J_{OH})_{closed} = -\frac{c_{OH} D_{OH}}{RT} \left(\frac{d\mu_{OH}}{dx} \right), \quad (14)$$

$$(J_V)_{closed} = -\frac{c_V D_V}{RT} \left(\frac{d\mu_V}{dx} \right). \quad (15)$$

By analogy with the open-circuit case, fluxes can be expressed as functions of the H_2 and H_2O virtual partial pressure gradients within the membrane and then re-arranged to give

$$\frac{d(\ln \pi_{H_2})}{d\xi} = -\frac{2j_{OH}}{\varepsilon_{OH}}, \quad (16)$$

$$\frac{d(\ln \pi_w)}{d\xi} = \frac{j_V}{\varepsilon_V \gamma_V} - \frac{2j_{OH}}{\varepsilon_{OH}}. \quad (17)$$

Eqs. (16) and (17) can then be integrated in order to obtain the fluxes, after applying appropriate boundary conditions

and introducing a relation between charge carrier concentrations (c_V and c_H) and gas-phase concentrations (p_{H_2} , p_w).

2.3. Electrochemical pumping

The membrane system can also be operated as an electrochemical pump by applying a direct voltage across the two sides. In this case, Eqs. (8) and (9) are required in order to describe the flux. Comparing Eqs. (8) and (9) with Eqs. (10) and (11) and defining the transference numbers for protons (t_{OH}), vacancies (t_V), and electron/holes (t_{el}) as

$$t_{OH} = \frac{c_{OH}D_{OH}}{A} = \frac{\varepsilon_{OH}}{\lambda}, \quad (18)$$

$$t_V = \frac{c_V D_V}{A} = \frac{\gamma_V \varepsilon_V}{\lambda}, \quad (19)$$

$$t_{el} = \frac{c_e D_e + c_h D_h}{A} = \frac{\gamma_e \varepsilon_e + \gamma_h \varepsilon_h}{\lambda}, \quad (20)$$

the fluxes across the membrane become

$$j_{OH} = t_{OH}i + (j_{OH})_{open} \quad (21)$$

$$j_V = t_V i + (j_V)_{open} \quad (22)$$

In Eqs. (21) and (22), the first and second terms reflect mass transport driven by electrical potential gradients imposed by an external voltage and by chemical potential gradients imposed by different gas compositions in the two sides of the membrane, respectively. When proton transference numbers are independent of applied voltage, the flux depends linearly on the current i with a slope equal to t_{OH} and a y -intercept given by the open-circuit hydrogen flux at a given chemical potential gradient across the membrane. In many cases, the proton transference number depends on the applied voltage, because membrane materials are semiconductors, and the relationship between the flux j_{OH} and the current density i becomes non-linear (Iwahara, 1999; Li & Iglesia, 2001).

Fig. 1 shows the expected dependence of the hydrogen flux on the current across the membrane for different operating modes. The solid and dashed lines in Fig. 1 represent flux behavior for membranes with proton transference numbers of one and less than one, respectively. For open-circuit conditions, the proton flux for membranes with proton transference numbers near unity would be zero, corresponding to point O in Fig. 1. For proton transference numbers below unity, proton transfer will occur even under open-circuit conditions (point A in Fig. 1), but the total net current across the membrane is zero, because currents carried by protons and electrons are equal but opposite in direction. Under short-circuited condition, all electrons are transported via the external circuit, because its resistance is much smaller than that of the membrane. In this case, the net current across the membrane is equal to the proton current, and hydrogen permeation rates become independent of the proton transference number; the two lines which represent the flux for membranes with $t_{OH} = 1$ and < 1 cross at point B in Fig. 1.

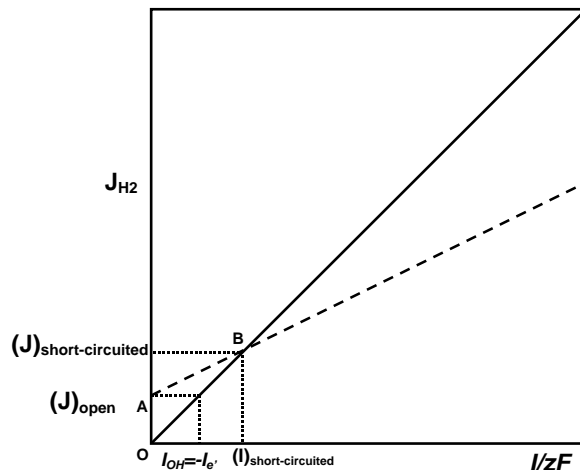


Fig. 1. Hydrogen flux under various operation modes. The solid and dashed lines represent the flux of membranes with $t_{OH} = 1$ and < 1 , respectively.

An external voltage can lead to higher proton fluxes. Eq. (21) shows that proton fluxes under electrochemical pumping conditions are linear functions of the current when t_{OH} is independent of applied voltage and the proton fluxes can become significantly greater than that under short-circuited conditions. A combination of hydrogen permeation rate measurements in these various operating modes can be used to determine the identity of the rate-controlling charge carriers and their respective electronic transference numbers. For example, comparisons of fluxes under open-circuit and short-circuited conditions give the average proton transference number t_{OH} (the slope of line AB in Fig. 1).

2.4. The relationship between fluxes of charge carriers (J_{OH} , J_V) and of molecules (J_{H_2} , J_w and J_{O_2})

In general, the motion of vacancies and protons leads to transport of H_2 , O_2 and H_2O across the membrane (the other two charge carriers, electrons and holes, do not directly contribute to the transport of molecular or atomic species). The specific origin of the proton cannot be rigorously established (from H_2 or H_2O) because of the H_2 – H_2O equilibrium. Vacancies can react with either O_2 or H_2O . However, the mass balance requires that

$$J_{OH} = 2J_{H_2} + 2J_w, \quad (23)$$

$$J_V = -2J_{O_2} - J_w. \quad (24)$$

The direction and magnitude of J_{H_2} , J_w and J_{O_2} depend on: (1) the chemical environment in each side of the membrane (e.g. H_2 , H_2O and O_2 pressures); (2) the membrane properties (the thermodynamics for reactions (4)–(7)); and (3) the mobility of charge carriers (D_V , D_{OH}) within the membrane material.

For selective hydrogen permeation, the transport rates of vacancies must be much lower than that of protons. Then, $J_V \approx 0$ and $J_w \approx 0$, and

$$J_{H_2} = 1/2 J_{OH}. \quad (25)$$

3. Charge carrier concentrations in mixed conductors

For mixed conductors, the gas-phase composition influences charge carrier concentrations and their gradients across the thickness of the membrane material. In order to rigorously account for these changes as a function of gas-phase environment and location within the membrane, we must relate the concentration of each charge carrier to one another and to the external environment at each membrane surface. Simulations of hydrogen permeation using the approach described above require that we estimate charge carrier concentrations as a function of H_2O and H_2 partial pressures.

For mixed conductors, these concentrations are obtained by considering the solid–gas reactions in Eqs. (4)–(7). In addition, electronic equilibrium requires that:

$$0 \stackrel{K_e}{=} h^{\cdot} + e, \quad (26)$$

and electrical neutrality imposes the additional constraint

$$2c_V + c_{OH} + c_h = c_{dopant} + c_e, \quad (27)$$

where c_{dopant} is the dopant concentration in the membrane. In $SrCe_{0.95}Yb_{0.05}O_{3-x}$ membrane, Yb acts as the dopant used in order to increase the electronic conduction of these materials.

The equilibrium between gas phase and membrane should be described using chemical potential, which poses a significant challenge. However, Kreuer (1999) proposed that interactions with gas-phase species can be described by assuming ideal behavior for all species involved in defect formation for cubic and distorted cubic perovskites. Therefore, we treated gas phase–membrane interaction as an ideal system, and we can then solve the concentrations of four charge carriers for a given set of H_2 and H_2O partial pressure by combining the equilibrium of Eqs. (4)–(7) with the electrical neutrality condition (Eq. (26)) (Appendix B).

The charge carrier concentrations depend on the equilibrium constants for reactions (4)–(7) and (26) (K_1 , K_2 , K_w and K_e) for a given membrane composition ($c_{dopant} = \text{constant}$) and temperature; they can be expressed in this manner as functions of p_{H_2} and p_w . Fig. 2 shows the concentrations of these four charge carriers with changes in p_{H_2} and p_w for $SrCe_{0.95}Yb_{0.05}O_{3-x}$ at 1000 K. The equilibrium constants, K_1 , K_2 , K_w and K_e reported by Schober, Friedrich, and Condon (1995) were used in these calculations. Water partial pressures influence proton concentrations more strongly than H_2 partial pressures, and the effect of the latter becomes more pronounced at high H_2 pressures ($p_{H_2} > 100$ Pa). In contrast, p_{H_2} strongly influences electron and hole concentrations over the entire range of

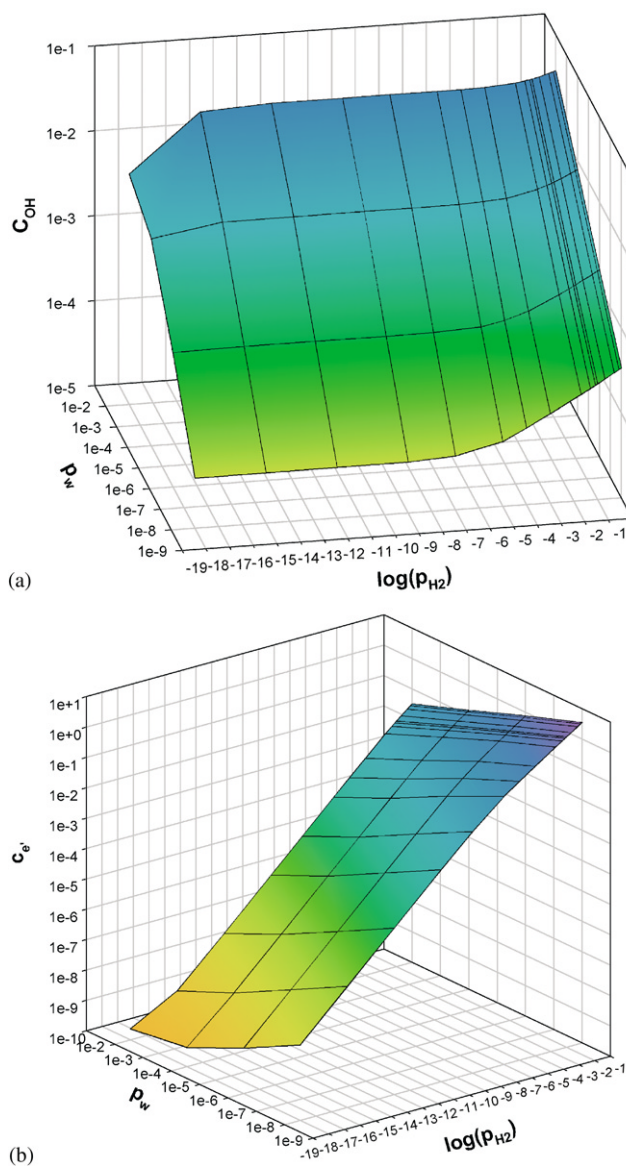


Fig. 2. Charge carrier concentration as functions of hydrogen and water partial pressure ($SrCe_{0.95}Yb_{0.05}O_{3-x}$, 1000 K): (a) proton concentration; (b) electron concentration; (c) hole concentration; and (d) vacancy concentration.

partial pressures. Electronic conduction is provided by electrons for reducing environments (high p_{H_2}) and by holes for less reducing conditions (low p_{H_2}). Therefore, the chemical composition of the gas streams influences not only the mass transfer driving force but also the charge carrier concentrations within the membrane, and hence the conductivities of charge carriers, as defined.

Conductivities are also influenced by the equilibrium constants, the values of which depend on the membrane material. For example, a higher value of K_2 indicates a higher membrane affinity for hydrogen, while higher K_1 values reflect higher membrane affinities for oxygen. By

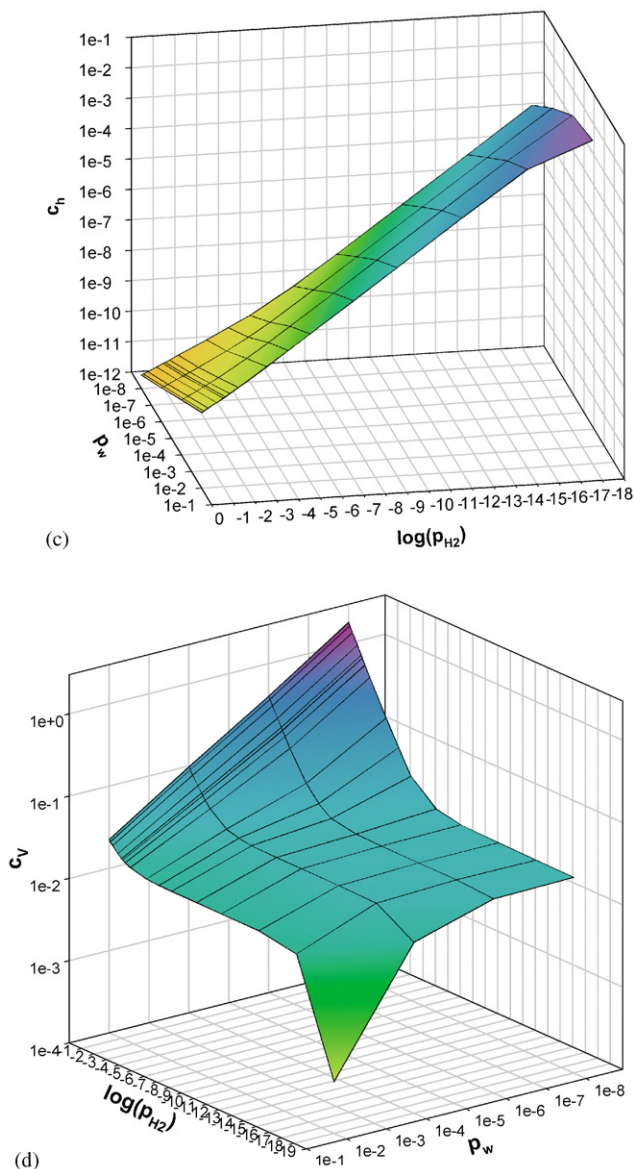


Fig. 2. continued.

incorporating the dependence of charge carrier concentrations on H_2 and H_2O partial pressures into the model equations derived in the previous section, hydrogen permeation rates can be predicted for mixed conducting membranes. The resulting simulations account rigorously for the effects of operating conditions on both the mass transfer driving force and the concentrations of charge carriers.

4. Simulation of hydrogen permeation behavior

For mixed conductors, the proton flux across the membrane is determined by the concentration and diffusivity of protons and by the electron transfer ability of the material, which is usually expressed as its electronic conductivity. As we will see later, the electronic conductivity is a function of

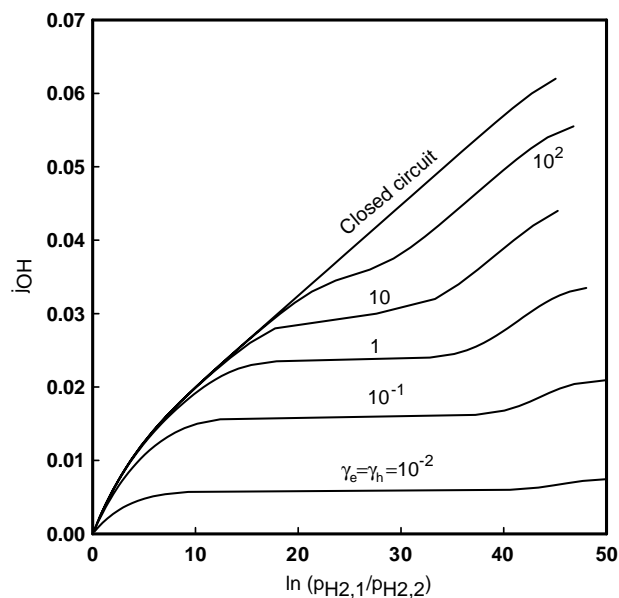


Fig. 3. Effect of electron/hole diffusivity on proton flux through $SrCe_{0.95}Yb_{0.05}O_{3-x}$ membrane; $p_{H_2,1} = 0.1$ MPa, $p_w = 10^{-6}$ MPa, $T = 950$ K.

position in the membrane because it depends on the electron concentration, which also varies with position. The effective electron-conducting ability of the membrane, which can be defined as an average electronic conductivity, depends on: (i) the concentrations of electrons and holes in the membrane and (ii) the diffusivities of electrons and holes. The concentrations of electrons and holes are determined by the properties of the materials (e.g., reducibility) and by the operating conditions. In this section, we examine the effects of membrane reducibility and diffusivity on proton fluxes.

Fig. 3 shows the effects of electron/hole diffusivity on proton flux under open-circuit and short-circuited conditions; the latter corresponds to very high electron/hole diffusivities (provided by the external circuit). For a given mass transfer driving force ($\ln(p_{H_2,1}/p_{H_2,2})$), the proton flux (j_{OH}) increases with increasing of electronic mobility, because charge neutrality requires the concurrent motion of protons and electron/holes. When γ_e and γ_h are very high ($> 10^2$), additional increases in electronic mobility do not influence H_2 permeation rates, because fluxes become limited by proton mobility.

The relationship between the proton flux (j_{OH}) and the chemical potential driving force for mass transfer $\{\ln(p_{H_2,1}/p_{H_2,2})\}$ depends on the electronic mobility of the membrane. In general, at low values of $\ln(p_{H_2,1}/p_{H_2,2})$ (< 5), both sides of the membrane are exposed to reducing mixtures (symmetric operating mode) and electronic conduction occurs predominately via electron transport. Higher $\ln(p_{H_2,1}/p_{H_2,2})$ values will lead to higher proton transport rates, because average electronic transference numbers will be largely independent of $\ln(p_{H_2,1}/p_{H_2,2})$. At sufficiently high $\ln(p_{H_2,1}/p_{H_2,2})$ values, however, the

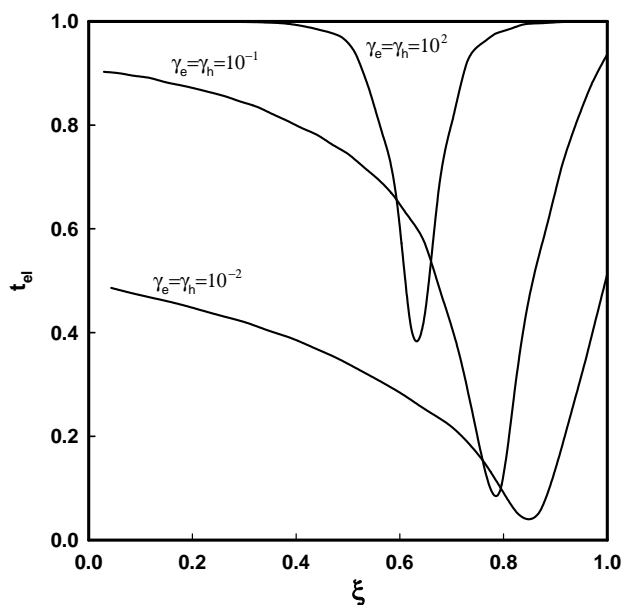


Fig. 4. Effect of electron/hole diffusivity on electronic transference number distribution inside membrane; $p_{\text{H}_2,1} = 0.1$ MPa, $p_w = 10^{-6}$ MPa, $T = 950$ K, $\ln(p_{\text{H}_2,1}/p_{\text{H}_2,2}) = 45$.

high oxygen activity in the permeate side leads to very low electron concentrations and to low average electronic transference numbers. As a result, the higher mass transfer driving force imposed by these high $\ln(p_{\text{H}_2,1}/p_{\text{H}_2,2})$ values will be partially offset by a concurrent decrease in the electronic transference number. Ultimately, high values of $\ln(p_{\text{H}_2,1}/p_{\text{H}_2,2})$ lead to an increase in the electronic transference number and to higher fluxes, because holes become the predominant charge carriers, at least in the membrane regions near the permeate side.

The effects of electron/hole diffusivity can also be examined by calculating electronic transference numbers (Eq. (20)) as a function of position within the membrane for asymmetrical conditions $\{\ln(p_{\text{H}_2,1}/p_{\text{H}_2,2}) = 45\}$. At these conditions, the membrane regions near the process side interact with a highly reducing environment and electrons are the predominant electronic carriers. As ξ increases, the virtual H_2 partial pressure decreases and the lower electron concentrations lead to lower electronic transference numbers. After reaching a minimum value, electronic transference numbers increase with increasing ξ because the permeate side is exposed to oxidizing conditions, which lead to higher hole concentrations and more effective electronic conduction. This conclusion is consistent with electronic conductivity measurements reported by Hamakawa, Hibino, and Iwahara (1994). Under asymmetrical conditions, there is a transition region within which t_{el} is very low and electron conduction determines the electronic conductivity and the hydrogen permeation rates. As the electron/hole mobility increases, the minimum t_{el} increases and the low t_{el} tran-

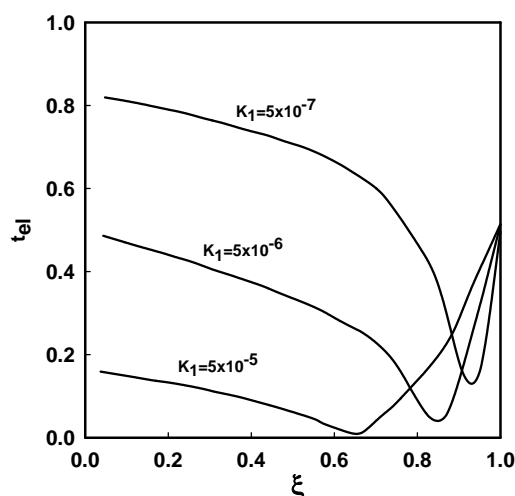


Fig. 5. Effect of reducibility (K_1) on electronic transference number distribution inside membrane; $p_{\text{H}_2,1} = 0.1$ MPa, $p_w = 10^{-6}$ MPa, $T = 950$ K, $\ln(p_{\text{H}_2,1}/p_{\text{H}_2,2}) = 45$, $\gamma_e = \gamma_h = 10^{-2}$, $\gamma_V = 10^{-5}$.

sition region becomes narrower; as a result, the average t_{el} for the membrane increases.

Symmetrical conditions lead to reducing environments throughout the membrane thickness and the t_{el} profile within the membrane is given by the left region in Fig. 4. Within this region, t_{el} decreases with increasing ξ because low H_2 virtual pressures lead to low concentrations of electrons; no increase in the electronic transference number is observed because the H_2 virtual pressure is never sufficiently low for holes to become the predominant charge carriers. The average t_{el} is higher than under asymmetrical conditions and the effects of varying the electronic conductivity or of closing an external circuit on proton fluxes are stronger for asymmetrical ($\ln(p_{\text{H}_2,1}/p_{\text{H}_2,2}) \sim 40$) than for symmetrical ($\ln(p_{\text{H}_2,1}/p_{\text{H}_2,2}) \sim 4$) conditions.

Our simulations also show that the effects of the chemical nature of the permeate stream depend on the membrane reducibility and on the mobility of charge carriers. When electronic mobility is low, hydrogen permeation rates are controlled by electronic conductivity. In this case, a shift from reducing to oxidizing conditions in the permeate side (symmetrical to asymmetrical modes) leads to small effects in permeation rates. When the electronic conductivity is high, either because of the properties of the membrane properties or because of an external circuit, more oxidizing environments in the permeate side lead to larger permeation rates, because the corresponding increase in permeation driving force is not offset by a concurrent decrease in electronic conductivity as a result of changes in the permeate stream.

The reducibility of the membrane material (given by K_1 in our model) also influences hydrogen permeation rates. Higher values of K_1 reflect stronger oxygen binding and less reducible membrane materials. Fig. 5 illustrates the effect of varying K_1 on the electronic transference number t_{el} . As K_1 increases, electronic transference numbers within the more

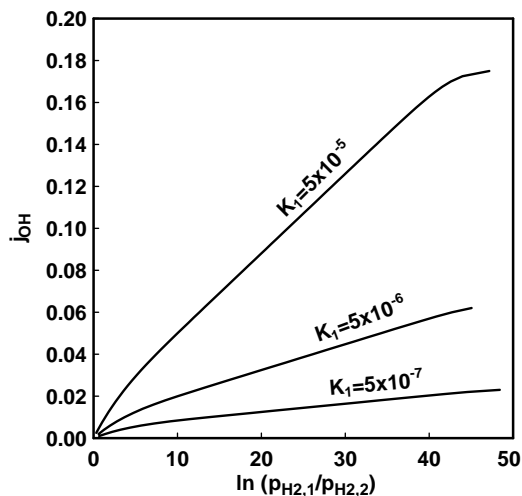


Fig. 6. Effect of reducibility on proton flux under short-circuited conditions; $p_{\text{H}_2,1} = 0.1$ MPa, $p_w = 10^{-6}$ MPa, $T = 950$ K.

reducing regions of the membrane (near the process side) decrease because of a decrease in electron concentrations. The location of the minimum electronic transference number moves towards the process side, suggesting that the region within which electrons are the dominant charge carriers becomes thinner. For the range of K_1 values we examined, the average t_{el} within the membrane decreases with decreasing of membrane reducibility. However, further increase of K_1 may lead to higher average t_{el} , because holes ultimately become the predominant charge carriers within a large fraction of the membrane thickness.

These findings suggest that for typical mixed conductors, such as $\text{SrCe}_{0.95}\text{Yb}_{0.05}\text{O}_{3-z}$, hydrogen permeation rates are largely controlled by electron conduction. Higher electronic conductivities will require higher concentrations or diffusivities of electrons or holes. In oxygen transport membranes, holes are the predominant charge carriers throughout the membrane thickness. In H_2 transport processes, at least one membrane surface is in contact with a strongly reducing environment; therefore, hole conduction cannot predominate throughout the entire membrane thickness. One potential solution is to increase electron concentration by selecting more reducible membrane materials. Reduction of membrane materials during operation, however, can lead to changes in the perovskite structure and to loss of mechanical integrity; thus, any such improvements in proton transport by increasing membrane reducibility is likely to be limited by these practical considerations.

In addition to its effects on electron/hole concentrations and t_{el} , the reducibility of the membrane also influences proton concentrations and hydrogen permeation rates. Figs. 6 and 7 show the effect of K_1 on proton flux under short-circuited and open-circuit operating modes, respectively. Under short-circuited conditions, j_{OH} increases with increasing of K_1 , and the sensitivity j_{OH} to the driving force term $\ln(p_{\text{H}_2,1}/p_{\text{H}_2,2})$ increases, indicating that a given mass

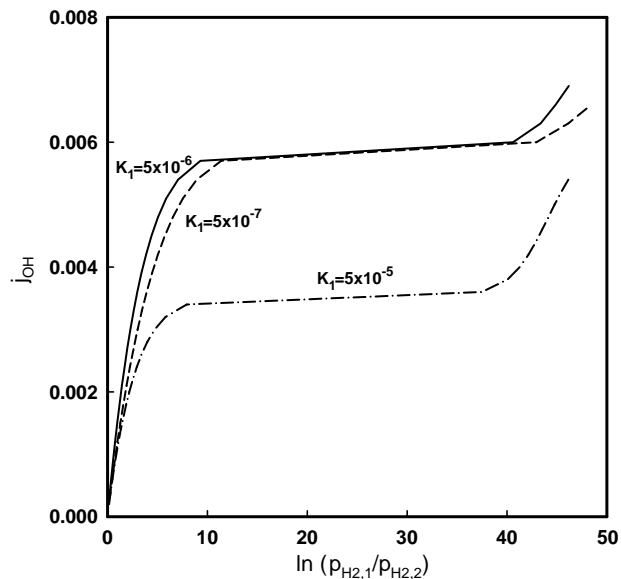


Fig. 7. Effect of reducibility on proton flux under open-circuit conditions; $p_{\text{H}_2,1} = 0.1$ MPa, $p_w = 10^{-6}$ MPa, $T = 950$ K, $\gamma_e = \gamma_h = 10^{-2}$, $\gamma_V = 10^{-5}$.

transfer driving force becomes more effective for H_2 transport as K_1 increases, because of the higher prevalent proton concentrations. In open-circuit mode, hydrogen permeation rates are largely controlled by electronic conduction. Therefore, higher values of K_1 lead to lower proton fluxes, as a result of the lower average electron concentrations prevalent as the membrane material becomes more difficult to reduce.

5. Usefulness and limitations of hydrogen transport model

The rigorous model presented here describes the transport properties of mixed conductors using the diffusivities and concentrations of each charge carrier as the fundamental relevant parameters responsible for net macroscopic motion. In doing so, it avoids the use of lumped phenomenological parameters, such as conductivities, which are appropriate for ideal electrical conductors, but not for the transport of chemical species through mixed conductors. The approach presented here also includes rigorous equilibria between the chemical environments in the process and permeate side and the defect species present at each membrane surface. As a result, the simulations implicitly contain the effects of these chemical environments on both the driving force for mass transfer and the concentrations of charge carriers.

One remaining issue, not currently treated in this model, is the potential effect of the chemical environment in the process and permeate side on the intrinsic mobility (diffusivity) of each charge carrier. Such effects may be important and difficult to measure, and they cannot be ruled out. We suggest, based on heuristic arguments and previous data, that they are not critical in determining transport rates. First, the concentrations of defects are small within typical membrane materials; therefore, non-idealities

arising from defect–defect interactions are unlikely to arise. Also, Yajima and Iwahara (1992a, b) have found that measured proton mobilities do not depend on proton concentrations for $\text{SrCe}_{0.95}\text{Yb}_{0.05}\text{O}_{3-x}$. When required, such effects must be described in terms of the atomic-level bond-making and bond-breaking mechanisms responsible for migration of hydrogen and oxygen species within such solids. Recent examples show the emerging feasibility of such fundamental approaches for all charge carriers in mixed conductors (Kreuer, 1996, 1997, 1999, 2000), but detailed knowledge of charge carrier transport within these solids remains very limited.

External boundary layer or surface adsorption resistances can easily be incorporated into the hydrogen permeation model described here. Both of these effects are occasionally important for oxygen transport membranes (Bouwmeester & Burggraaf, 1996). Boundary layer effects have been neglected here for H_2 transport membranes because H_2 molecules diffuse much more rapidly than O_2 molecules through a gas-phase boundary layer, while membrane permeation rates in practical applications are generally similar for both molecules. Dissociative chemisorption of H_2 is expected to occur more rapidly than for O_2 , because of the smaller bond energies in H_2 . Also, H_2 transport membranes must be operated below 1000 K in order to avoid oxygen transport and membrane over-reduction; as a result proton fluxes tend to be lower than for O_2 transport membranes, which operate at much higher temperatures (~ 1300 K). Finally, our recent studies have shown that even for very thin $\text{SrCe}_{0.95}\text{Yb}_{0.05}\text{O}_{3-x}$ ($< 10 \mu\text{m}$) films, the proton flux remains proportional to the inverse of the film thickness (Hamakawa, Li, Li, & Iglesia, 2002); thus, surface processes remain kinetically irrelevant even for very high H_2 permeation rates. In some sense, this reflects the lower permeation rates for H_2 in proton–electronic conductors at their typical temperatures (1 bar H_2 , 950 K; 5^{-3} S cm^{-1} for $\text{SrCe}_{0.95}\text{Yb}_{0.05}\text{O}_{3-x}$; Iwahara, 1996) than for O_2 in oxide–electronic conductors (0.2 bar O_2 , 1273 K, 0.5 S cm^{-1} ; Bouwmeester & Burggraaf, 1996). Thus, it appears that the inclusion of external transport and adsorption kinetics is not required for currently available proton mixed conductor membranes. As H_2 permeation rates continue to increase with advances in the hydrogen permeability of these materials, both external transport and H_2 chemisorption kinetics must be rigorously described in order to replace the equilibrium between the surface and the bulk fluid assumed within the current model.

6. Conclusions

A mass transfer model for hydrogen permeation through proton–electronic mixed conductors was developed by using the formalism of non-equilibrium thermodynamics and describing the concentrations of all charge carriers through equilibrium with the contacting gas phase at surfaces and

through a virtual pressure formalism within the membrane material. This model was used to describe H_2 permeation through dense $\text{SrCe}_{0.95}\text{Yb}_{0.05}\text{O}_{3-x}$ membranes. These simulations confirmed the rate-controlling role of electronic transport in H_2 permeation processes, especially when the membrane is operated at very different hydrogen chemical potentials in the process and the permeate sides. Under such asymmetric operating conditions, an internal region with very low electronic transference number arises from a transition from electronic to hole conduction as the hydrogen chemical potential within the membrane decreases from high values near the process side to much lower values near the permeate side. As a result, when electronic mobility is high, either because of the nature of the membrane material or because of the presence of an external conducting circuit, large H_2 chemical potential gradients across the membrane exploit the full driving force without the adverse effects of the lower electronic transport rates associated with such chemical potential gradients. When electronic transport limits H_2 permeation rates, the full effects of these large chemical potential gradients cannot be exploited, because of their negative effects on electron transport rates. Improvements in electronic (and H_2) transport rates require higher electron/hole diffusivities or more reducible membrane materials, which increase electron concentrations for a given chemical environment. Simulation results illustrate the nature and the underlying mechanism for the observed effects of the chemical environment in each side of the membrane on H_2 permeation rates and how such effects depend on membrane properties, such as reducibility and charge carrier mobility. Heuristic arguments and experimental results are used to neglect the effects of external mass transport and of H_2 dissociation rates on the rate of H_2 permeation through typical mixed proton–electronic conductors. These external transport and adsorption effects can be readily incorporated into the current framework when the experimental situation requires it.

Notation

c_h	concentration of charge carrier k , mol m^{-3}
C_T	molar concentration of membrane (given by membrane density divided by molecular weight), mol m^{-3}
D_k	diffusivity of charge carrier k , $\text{m}^2 \text{ s}^{-1}$
F	Faraday constant C mol^{-1}
i	Dimensionless current density
I	total current density, A m^{-2}
I_k	current density carried by charge k , A m^{-2}
j_k	dimensionless flux of component k , defined by Eqs. (A.19) and (A.20)
J_k	flux of component k , $\text{mol m}^{-2} \text{ s}^{-1}$
K_i	equilibrium constant, defined by Eqs. (B.1)–(B.4)
L	membrane thickness, m
p_k	partial pressure of component k , Pa

t_k	transference number of charge carrier k
x	distance along membrane thickness, m
z_k	charge on species k

Greek letters

γ_k	dimensionless mobility of charge carrier k , defined by Eqs. (A.22)–(A.24)
ε_k	dimensionless concentration of charge carrier k , defined by Eqs. (A.25)–(A.28)
η_k	electrochemical potential of species k , J mol ⁻¹
λ	defined by Eq. (A.30)
A	defined by Eq. (3)
μ_k	chemical potential of species k , J mol ⁻¹
ξ	dimensionless distance, $\xi = x/L$
π_k	virtual partial pressure of component k , Pa
ϕ	electrical potential, V

Subscripts

h	holes
e	electrons
OH	proton defect
V	vacancy
w	water

Acknowledgements

This work was supported by the Division of Fossil Energy of the U.S. Department of Energy (Contract No. DE-AC03-76SF00098) under the technical supervision of Dr. Daniel Driscoll.

Appendix A. Derivation of flux equations under various conditions

In mixed conductors, both chemical and electrical potential gradients can exist and act as the driving force for mass transport. In one dimension (x =membrane thickness dimension), the mass transfer rate per cross-sectional area (flux) of component k is given by (Bouwmeester & Burggraaf, 1996)

$$J_k = -\frac{c_k D_k}{RT} \frac{d\eta_k}{dx}, \quad (\text{A.1})$$

where η_k , the electrochemical potential of component k , contains both the chemical (μ_k) and the electrical potentials (ϕ) driving the transport of molecules across the membrane:

$$\eta_k = \mu_k + z_k F \phi. \quad (\text{A.2})$$

Substituting Eq. (A.2) into Eq. (A.1), we obtain Eq. (1).

The charge current carried by component k is

$$I_k = z_k F J_k, \quad (\text{A.3})$$

and the total current across the membrane is given by

$$I = \sum_{k=1}^n I_k = I_1 + \sum_{k=2}^n z_k F J_k. \quad (\text{A.4})$$

Substituting the expression for J_k into Eq. (1), we obtain

$$\sum_{k=2}^n z_k J_k = -\sum_{k=2}^n \frac{c_k D_k z_k}{RT} \frac{d\mu_k}{dx} - \sum_{k=2}^n \frac{c_k D_k z_k^2}{RT} F \frac{d\phi}{dx}, \quad (\text{A.5})$$

and rearranging provides an expression for the electrical potential gradient:

$$F \frac{d\phi}{dx} = \frac{\sum_{k=2}^n z_k J_k + \sum_{k=2}^n \frac{c_k D_k z_k^2}{RT} \frac{d\mu_k}{dx}}{-\sum_{k=2}^n \frac{c_k D_k z_k^2}{RT}}. \quad (\text{A.6})$$

Substituting Eqs. (A.3), (A.4), and (A.6) into Eq. (1) we obtain Eq. (2).

From Eqs. (4)–(7),

$$\mu_{\text{H}_2} = 2\mu_{\text{OH}} + 2\mu_e, \quad (\text{A.7})$$

$$1/2\mu_{\text{O}_2} + \mu_V = 2\mu_h, \quad (\text{A.8})$$

$$\mu_w + \mu_V = 2\mu_{\text{OH}}, \quad (\text{A.9})$$

$$\mu_{\text{H}_2} + 1/2\mu_{\text{O}_2} = \mu_w. \quad (\text{A.10})$$

Based on Eqs. (A.7)–(A.10), the flux equations can be expressed as functions of gradients of chemical potential of hydrogen and water:

$$J_{\text{OH}} = \frac{c_{\text{OH}} D_{\text{OH}}}{A} \frac{I}{F} - \frac{c_{\text{OH}} D_{\text{OH}}}{ART} \times \left[(c_h D_h + c_e D_e) \frac{1}{2} \frac{d\mu_{\text{H}_2}}{dx} + 2c_V D_V \frac{d\mu_w}{dx} \right], \quad (\text{A.11})$$

$$J_V = \frac{2c_V D_V}{A} \frac{I}{F} + \frac{c_V D_V}{ART} \left[(c_h D_h + c_e D_e + c_{\text{OH}} D_{\text{OH}}) \times \frac{d\mu_w}{dx} - (c_h D_h + c_e D_e) \frac{d\mu_{\text{H}_2}}{dx} \right]. \quad (\text{A.12})$$

The chemical potential of H₂ and H₂O can be calculated in terms of their respective virtual pressures:

$$\mu_{\text{H}_2(g)} = \mu_{\text{H}_2}^0 + RT \ln(\pi_{\text{H}_2}), \quad (\text{A.13})$$

$$\mu_{\text{w}(g)} = \mu_w^0 + RT \ln(\pi_w), \quad (\text{A.14})$$

$$\frac{d\mu_{\text{H}_2}}{dx} = RT \frac{1}{\pi_{\text{H}_2}} \frac{d\pi_{\text{H}_2}}{dx}, \quad (\text{A.15})$$

$$\frac{d\mu_w}{dx} = RT \frac{1}{\pi_w} \frac{d\pi_w}{dx}. \quad (\text{A.16})$$

Then the flux equations can be expressed as functions of hydrogen and water partial pressure gradients:

$$J_{\text{OH}} = \frac{c_{\text{OH}}D_{\text{OH}}}{A} \frac{I}{F} - \frac{c_{\text{OH}}D_{\text{OH}}}{2A} \left[(c_h D_h + c_e D_e) \times \frac{1}{\pi_{\text{H}_2}} \frac{d\pi_{\text{H}_2}}{dx} + 4c_V D_V \frac{1}{\pi_w} \frac{d\pi_w}{dx} \right], \quad (\text{A.17})$$

$$J_V = \frac{2c_V D_V}{A} \frac{I}{F} + \frac{c_V D_V}{A} \left[(c_h D_h + c_e D_e + c_{\text{OH}} D_{\text{OH}}) \frac{1}{\pi_w} \times \frac{d\pi_w}{dx} - (c_h D_h + c_e D_e) \frac{1}{\pi_{\text{H}_2}} \frac{d\pi_{\text{H}_2}}{dx} \right]. \quad (\text{A.18})$$

Eqs. (A.17) and (A.18) can be nondimensionlized to Eqs. (8) and (9) by defining

$$j_H = \frac{J_{\text{OH}} L}{C_T D_{\text{OH}}}, \quad (\text{A.19})$$

$$j_V = \frac{J_V L}{C_T D_{\text{OH}}}, \quad (\text{A.20})$$

$$i = \frac{IL}{C_T D_{\text{OH}} F}, \quad (\text{A.21})$$

$$\gamma_h = D_h / D_{\text{OH}}, \quad (\text{A.22})$$

$$\gamma_e = D_e / D_{\text{OH}}, \quad (\text{A.23})$$

$$\gamma_V = D_V / D_{\text{OH}}, \quad (\text{A.24})$$

$$\varepsilon_h = c_h / C_T, \quad (\text{A.25})$$

$$\varepsilon_e = c_e / C_T, \quad (\text{A.26})$$

$$\varepsilon_V = c_V / C_T, \quad (\text{A.27})$$

$$\varepsilon_{\text{OH}} = c_{\text{OH}} / C_T, \quad (\text{A.28})$$

$$\xi = x / L, \quad (\text{A.29})$$

$$\lambda = A / (C_T D_{\text{OH}}) = \varepsilon_h \gamma_h + \varepsilon_e \gamma_e + \varepsilon_{\text{OH}} + 4\varepsilon_V \gamma_V, \quad (\text{A.30})$$

where L the membrane thickness and C_T is the mole concentration of the membrane.

For short-circuited conditions, using Eqs. (A.13)–(A.16), Eqs. (14) and (15) can be expressed as

$$(J_{\text{OH}})_{\text{closed}} = -\frac{c_{\text{OH}} D_{\text{OH}}}{2\pi_{\text{H}_2}} \frac{d\pi_{\text{H}_2}}{dx}, \quad (\text{A.31})$$

$$(J_V)_{\text{closed}} = \frac{c_V D_V}{\pi_w} \frac{d\pi_w}{dx} - \frac{c_V D_V}{\pi_{\text{H}_2}} \frac{d\pi_{\text{H}_2}}{dx}. \quad (\text{A.32})$$

The above equations can be non-dimensionlized as

$$(j_{\text{OH}})_{\text{closed}} = \frac{\varepsilon_{\text{OH}}}{2} \frac{d \ln(\pi_{\text{H}_2})}{d\xi}, \quad (\text{A.33})$$

$$(j_V)_{\text{closed}} = \varepsilon_V \gamma_V \frac{d \ln(\pi_w)}{d\xi} - \varepsilon_V \gamma_V \frac{d \ln(\pi_{\text{H}_2})}{d\xi}. \quad (\text{A.34})$$

Eqs. (A.33) and (A.34) can be rearranged to give Eqs. (16) and (17).

Appendix B. Calculation of charge carrier concentrations

The corresponding equilibrium expressions for reactions (4)–(7) and (26) are given by

$$K_1 = c_h^2 / c_V p_{\text{O}_2}^{1/2}, \quad (\text{B.1})$$

$$K_2 = c_{\text{OH}}^2 c_e^2 / p_{\text{H}_2}, \quad (\text{B.2})$$

$$K_w = p_w / p_{\text{H}_2} p_{\text{O}_2}^{1/2}, \quad (\text{B.3})$$

$$K_e = c_h c_e. \quad (\text{B.4})$$

Based on Eqs. (B.1)–(B.4), a non-linear equation is obtained for the proton concentration within the membrane:

$$c_{\text{OH}}^3 + a c_{\text{OH}}^2 + b c_{\text{OH}} + c = 0, \quad (\text{B.5})$$

where

$$a = \frac{K_1 K_2 p_{\text{H}_2} p_{\text{O}_2}^{1/2}}{2K_e^2} + \frac{K_1 p_{\text{O}_2}^{1/2} \sqrt{K_2 p_{\text{H}_2}}}{2K_e}, \quad (\text{B.6})$$

$$b = -c_{\text{dopant}} \frac{K_1 K_2 p_{\text{H}_2} p_{\text{O}_2}^{1/2}}{2K_e^2}, \quad (\text{B.7})$$

$$c = -\frac{K_1 p_{\text{O}_2}^{1/2} (K_2 p_{\text{H}_2})^{3/2}}{2K_e^2}. \quad (\text{B.8})$$

Then,

$$c_e = \frac{\sqrt{K_2 p_{\text{H}_2}}}{c_{\text{OH}}}, \quad (\text{B.9})$$

$$c_h = \frac{K_e c_{\text{OH}}}{\sqrt{K_2 p_{\text{H}_2}}}, \quad (\text{B.10})$$

$$c_V = \frac{K_e^2 c_{\text{OH}}}{K_2 p_{\text{H}_2} K_1 p_{\text{O}_2}^{1/2}}. \quad (\text{B.11})$$

References

- Balachandran, U., Lee, T. H., Zhang, G., Dorris, S. E., Rothenberger, K. S., Howard, B. H., Morreale, B., Cugini, A. V., Siriwardane, R. V., Poston Jr., J. A., & Fisher, E. P. (2001). Development of dense ceramic membranes for hydrogen separation. *Studies in Surface Science and Catalysis*, 136, 465–470.
- Boudart, M., & Djega-Mariadassou, G. (1984). *Kinetics of heterogeneous catalytic reactions*. Princeton, NJ: Princeton University Press.

- Bouwmeester, H. J., & Burggraaf, A. J. (1996). In A. J. Burggraaf (Ed.), *Fundamentals of inorganic membrane science and technology* (pp. 435–528). Amsterdam: Elsevier Science.
- Guan, J., Dorris, S. E., Balachandran, U., & Liu, M. (1998). Transport properties of $\text{SrCe}_{0.05}\text{Y}_{0.95}$ and its application for hydrogen separation. *Solid State Ionics*, *110*, 303–310.
- Hamakawa, S., Hibino, T., & Iwahara, H. (1994). Electrochemical hydrogen permeation in a proton-hole mixed conductor and its application to a membrane reactor. *Journal of the Electrochemical Society*, *141*, 1720–1725.
- Hamakawa, S., Li, L., Li, A., & Iglesia, E. (2002). Synthesis and hydrogen permeation properties of membranes based on dense $\text{SrCe}_{0.95}\text{Yb}_{0.05}\text{O}_3$ thin films. *Solid State Ionics*, *48*, 71–81.
- Huggins, R. (2001). Use of defect equilibrium diagrams to understand minority species transport in solid electrolyte. *Solid State Ionics*, *143*, 3–16.
- Iwahara, H. (1996). Proton conducting ceramics and their applications. *Solid State Ionics*, *86–88*, 9–15.
- Iwahara, H. (1999). Hydrogen pumps using proton-conducting ceramics and their applications. *Solid State Ionics*, *125*, 271–278.
- Kreuer, K. D. (1996). Proton conductivity: materials and applications. *Chemical Letter*, *8*, 610–641.
- Kreuer, K. D. (1997). On the development of proton conducting materials for technological application. *Solid State Ionics*, *97*, 1–15.
- Kreuer, K. D. (1999). Aspects of formation and mobility of protonic charge carriers and the stability of perovskite-type oxides. *Solid State Ionics*, *125*, 285–302.
- Kreuer, K. D. (2000). On the complexity of proton conduction phenomena. *Solid State Ionics*, *136–137*, 149–160.
- Li, L., & Iglesia, E. (2001). Synthesis and characterization of proton-conducting oxides as hydrogen transport membranes. *Studies in Surface Science and Catalysis*, *136*, 357–362.
- Norby, T. (1999). Solid-state protonic conductors: Principles, properties, progress and prospects. *Solid State Ionics*, *125*, 1–11.
- Norby, T., & Larring, Y. (2000). Mixed hydrogen ion–electronic conductors for hydrogen permeable membranes. *Solid State Ionics*, *136–137*, 139–148.
- Nowick, A. S., & Du, Y. (1996). High-temperature protonic conductor with perovskite-related structure. *Solid State Ionics*, *77*, 137–146.
- Qi, X., & Lin, Y. S. (2000). Electrical conduction and hydrogen permeation through mixed proton–electron conducting strontium cerate membranes. *Solid State Ionics*, *130*, 149–156.
- Schober, T., Friedrich, J., & Condon, J. B. (1995). Effective hydrogen diffusivity in $\text{SrCe}_{0.95}\text{Yb}_{0.05}\text{O}_{3-x}$ and $\text{SrZr}_{0.95}\text{Yb}_{0.05}\text{O}_{3-x}$. *Solid State Ionics*, *75*, 175–179.
- Schober, T., Schilling, W., & Wenzl, H. (1996). Defect model of proton insertion into oxides. *Solid State Ionics*, *86–88*, 653–658.
- Smyth, D. M. (1992). Oxidative nonstoichiometry in Perovskite oxides. In L. G. Tejuca, & J. L. G. Fierro (Eds.), *Properties and applications of Perovskite-type oxides* (pp. 47–72). New York: Marcel Dekker.
- Tuller, H. L. (1981). Mixed conduction in nonstoichiometric oxides. In O. T. Sorensen (Ed.), *Nonstoichiometric oxides* (pp. 271–325). New York: Academic Press.
- Yajima, T., & Iwahara, H. (1992a). Studies on proton behavior in doped perovskite-type oxides: (I). *Solid State Ionics*, *50*, 281.
- Yajima, T., & Iwahara, H. (1992b). Studies on proton behavior in doped perovskite-type oxides: (II) Dependence of equilibrium hydrogen concentration and mobility on dopant content in Yb doped SrCeO_3 . *Solid State Ionics*, *53–56*, 983–988.